Supplement of Atmos. Chem. Phys., 19, 5127–5145, 2019
https://doi.org/10.5194/acp-19-5127-2019-supplement

Atmospheric Chemistry and Physics
Open Access
EGU

Supplement of

Intercomparison of O_3 formation and radical chemistry in the past decade at a suburban site in Hong Kong

Xufei Liu et al.

Correspondence to: Hai Guo (ceguohai@polyu.edu.hk)

Text S1. Determinations of the locally-produced and regionally-transported O_3 and discussions on the uncertainties.

As an observation based mode, PBM-MCM has been widely used to simulate the in-situ O_3 production (Lam et al., 2013; Ling et al., 2014; Lyu et al., 2017b; Y. Wang et al., 2017). Therefore, the O_3 simulated by PBM-MCM can be regarded as the locally-produced O_3, and the differences between the observed and simulated O_3 were taken as the regionally-transported O_3. However, it should be noted that the observed concentrations of O_3 precursors could be partially built up by regional transport. For example, under the northwest winds, the average mixing ratios of CO (693.9±25.5 ppbv), ethyne (2.15±0.22 ppbv), ethane (2.31±0.25 ppbv), propane (2.97±0.51 ppbv) and toluene (2.42±0.52 ppbv) were the highest among all the wind sectors. Since the PBM-MCM was constrained by the observed concentrations of O_3 precursors, the share of regionally-transported O_3 precursors in the observations made contributions to the simulated O_3, which in fact represented a kind of regional transport. Therefore, the locally produced O_3 were to some extent overestimated in this way. Conversely, the regionally-transported O_3 were underestimated. However, it is difficult to accurately quantify the contributions of regional transport to O_3 precursors at the site, and also due to the non-linear relationships between O_3 and its precursors, we did not quantitatively evaluate the overestimation of the locally-produced O_3 and the underestimation of the regionally-transported O_3.

Text S2. Set-up of the simulation scenarios

The base scenario (scenario A) was established to simulate the local production of O_3, with the observed concentrations of air pollutants (excluding O_3) as model inputs. The observed O_3 was not input because the simulated O_3 would be constrained to the observed values with the outputs exactly the same as the inputs otherwise. The scenario B was established to simulate

O_3 under the assumption that a source of VOCs was totally removed. Namely, the VOCs emitted from a specific source were subtracted from the observed VOCs when allocating the model inputs. In this study, six sources of VOCs were identified (see section 3.4.1). Therefore, 6 sub-scenarios were included in scenario B, because the VOCs emitted from the individual sources were subtracted one by one. In this approach, the differences in simulated O_3 between scenario A and scenario B were the contributions of individual VOC sources to the local O_3 production.

Text S3. Uncertainties in HONO concentrations adopted in model simulations and the subsequent uncertainties in the contributions of HONO to OH formation and loss rates.

To evaluate the uncertainties of adopting the HONO concentrations in 2011 in the model, we calculated the average diurnal cycles of HONO in the 2007, 2013 and 2016 sampling campaigns (Figure S5), according to the diurnal patterns of HONO/NO_x ratios determined at the same site (Xu et al., 2015). It was found that by adopting the values in 2011, the HONO concentrations were underestimated by 14.9% and 11.6% in 2007 and 2013, respectively, but were overestimated by 10.4% 2016. Further, the sensitivity tests indicated that the maximum underestimation (overestimation) of the total OH production rate was 2.3±2.3% (21.6±5.2%) in 2007, 5.8±1.3% (3.4±1.0%) in 2013 and 5.7±1.3% (3.4±0.9%) in 2016. It should be noted that the maximum overestimation of the total OH production rate in 2007 (21.6±5.2%) occurred at 07:00 LT when the OH recycling was weak. During 08:00 – 19:00 LT, both the underestimation and overestimation of the simulated total OH production rates were less than 3%. Therefore, it was concluded that the simulated OH formation and loss rates were not largely biased by adopting the measured HONO at TC in 2011 in all the simulations.

Besides, the HONO concentrations calculated from the HONO/NO_x ratios and NO_x concentrations also had certain uncertainties. Thus, we did not use the calculated HONO

concentrations to constrain the model. In fact, the consistent input of the diurnal cycle of HONO concentrations in the three sampling campaigns enabled us to look into the changes of O_3 and radical photochemistry induced by the other factors, such as VOCs, NO_x and meteorological conditions.

Table S1. Summary of the representative studies regarding O_3 pollution in Hong Kong.

Reference	Site	Measurement period	Nature of monitoring	Target	Main conclusions
Cheng et al, 2010	Wanqingsha (WQS), Guangdong and Tung Chung (TC), Hong Kong	Oct-Dec 2007	Suburban	O_3	O_3 formation was limited by VOCs at both sites. Carbonyls played important roles in photochemistry.
Cheng et al, 2013	TC, HK	Sep 2007 and Sep 2008	Suburban	O_3, VOCs	Major sources of VOCs in HK included consumer products, paint and printing solvent, road transport, and industrial, commercial, domestic and off-road transport.
Ding et al, 2004	PRD	Sep 2001	Large area	O_3	O_3 pollution events in PRD were close associated with sea-land breezes and tropical cyclones.
Guo et al, 2011	WQS and TC	Oct-Dec 2007	Suburban	VOCs	Solvent use, vehicular emissions, biomass burning, LPG usage and gasoline evaporation dominated the sources of VOCs in PRD.
Guo et al, 2013a	Tsuen Wan (TW) and Tai Mao Shan (TMS), HK	Sep-Nov 2010	TW: Urban TMS: Mountainous	O_3	Less NO titration, vertical transport, valley breeze and regional transport caused higher O_3 at the mountainous site.
Huang et al, 2005	HK	1999-2003	Large area	O_3	Tropical cyclones, continental anticyclones and troughs were conducive to O_3 pollution events in Hong Kong.
Lam et al, 2005	TC, HK	Aug 1999	Suburban	O_3, VOCs	Local thermal circulation under calm synoptic conditions trapped air pollutants, resulting in O_3 enhancements in HK.
Ling et al, 2013	TC, HK	Sep-Nov 2010	Suburban	O_3	High O_3 in HK was a combined effect of both local formation and regional transport
Ling et al, 2014	TW and TMS, HK	Sep-Nov 2010	TW: Urban TMS: Mountainous	O_3	Different O_3 production and destruction pathways at two sites. More aged air masses at the mountainous site favored O_3 formation.
Lyu et al, 2016a	Multiple, HK	Sep 2013 and Sep 2014	Urban Suburban Rural	VOCs	VOCs emitted from LPG-fueled vehicles significantly decreased at urban roadside sites. O_3 formation was limited by VOCs regardless of locations, while VOCs and NO_x co-limited O_3 formation in rural areas.
Lyu et al, 2016b	Mong Kok (MK), HK	Jun 2011-May 2014	Roadside	O_3, VOCs	Replacing catalytic converters in LPG-fueled vehicles led to substantial reductions of VOCs and NO_x emissions.
Lyu et al, 2017a	TC, HK	2005-2013	Suburban	VOCs	VOCs emitted from solvent usage and diesel exhaust decreased in Hong Kong from 2005 to 2013.

Ou et al, 2015	TC, HK	2005-2013	Suburban	VOCs	Vehicular exhaust, gasoline evaporation and LPG usage, consumer product and printing, architectural paints, and biogenic emissions were identified as the sources of VOCs in the study area.
So and Wang, 2003	Multiple, HK	Jun 1999-May 2000	Urban Suburban Rural	O_3	Air quality in rural areas was frequently influenced by regional air masses, while was predominantly affected by local emissions in urban areas.
Y. Wang et al, 2017	TC, HK	2005-2014	Suburban	O_3	Locally produced autumn O_3 decreased in Hong Kong, which was reversed by regionally-transported O_3 between 2005 and 2013.
Y. Wang et al, 2018	Wan Shan Island (WSI), GD	Aug-Nov 2013	Rural	O_3	O_3 formation switched from the NO_x-limited regime on low O_3 days to VOC-limited regime on high O_3 days over South China Sea.
Xu et al, 2008	Linan, Zhejiang	Aug 1991-Jul 2006	Rural	O_3	Monthly highest 5% of O_3 increased from 1991 to 2006, with enhanced variability, likely due to the increased NO_x emissions.
Xue et al, 2014a	TC, HK	Sep-Nov of 2002-2013	Suburban	O_3	Increase of regionally-transported O_3 offset the decrease of locally-produced O_3 and resulted in the increase of observed O_3 in the autumn in HK during 2002-2013.
Zhang et al, 2007	Multiple, HK	Oct-Dec 2002	Urban Suburban Rural	O_3	50-100% of O_3 enhancement during O_3 episodes in HK was explained by local photochemical formation, following the oxidation of anthropogenic VOCs.

Table S1. Summary of the sampling periods, VOC sampling dates and number of samples in the 2007, 2013 and 2016 sampling campaigns.

Year	Sampling period	Month	Date	Number of NMHC samples	Number of OVOC samples
2007	23 Oct.–1 Dec.	Oct.	26-27	96	28
		Nov.	13, 15-17, 23		
		Dec.	1		
2013	11 Aug.–22 Nov.	Sept.	11-12, 26	146	124
		Oct.	2-4, 9-10, 17, 22-25, 30-31		
		Nov.	15, 19-21		
2016	25 Sept. – 29 Nov.	Sept.	26	172	123
		Oct.	14-17, 23, 31		
		Nov.	1-7,14-18		
Total				414	275

Table S3. Instruments, analysis techniques, detection limits and time resolutions for the real-

time measurements of trace gases at the TC air quality monitoring station.

Species	Instrument	Analysis technique	Detection limit	Time resolution
SO_2	API 100E	UV fluorescence	0.4 ppb	1 sec
CO	API 300	Non-dispersive infra-red absorption with gas filter correlation	<0.050 ppm	1 sec
NO-NO_2-NO_x	API 200A	Chemiluminescence	0.4 ppb	1 sec
O_3	API 400	UV absorption	0.6 ppb	1 sec

Table S4. Summary of limits of detection (LoDs), precisions and accuracies of the GC-MSD/FID/ECD systems used for NMHCs analyses of whole air samples collected in 2007, 2013 and 2016 (Simpson et al., 2010; Y. Wang et al., 2018).

Institution	Year	Limit of Detection	Precision	Accuracy
UCI	2007	3-10 pptv	3%	5%
GIG	2013	3-57 pptv	2-5%	5%
HKPolyU	2016	3-10 pptv	5%	5%

Table S5. Statistics of VOC mixing ratios measured in 2007, 2013 and 2016. The 95% C.I., Max. and S.D. denote the 95% confidence interval, maximum and standard deviation of the mixing ratios of VOC species, respectively (Unit: pptv).

VOC species	2007			2013			2016		
	Mean±95%CI	Max.	S.D.	Mean±95%CI	Max.	S.D.	Mean±95%CI	Max.	S.D.
Ethane	1587.6±37.3	1994.6	186.7	1918.9±140.1	5700.4	1123.4	1729.1±85.3	3951.2	655.6
Ethene	1388.7±53.5	2284.7	267.3	1074.9±94.3	4529.8	751.9	886.8±79.1	4335.5	605.3
Ethyne	1939.3±105.3	3855.4	526.3	1563.4±94.8	3339.0	760.0	1399.2±83.1	4254.7	637.5
Propane	2826.2±94.1	3889.6	472.0	1619.1±110.4	5826.3	883.4	2308.4±224.2	13269.8	1715.9
Propene	325.2±34.0	1036.7	169.9	296.1±20.3	1052.3	162.7	192.3±13.8	773.6	105.5
i-Butane	790.9±40.7	1269.3	203.6	1556.4±115.5	5778.5	922.7	901.5±67.5	3229.9	516.6
n-Butane	1562.4±124.3	3360.3	621.5	1402.6±95.8	5353.7	767.8	1403.8±116.3	5001.2	893.8
1-/i-Butene	275.1±71.2	2945.2	356.1	240.7±70.6	5944.6	566.2	98.0±9.4	715.8	71.7
trans-2-Butene	22.5±6.0	213.4	29.7	31.2±6.7	387.1	42.5	12.1±2.9	184.1	18.3
cis-2-Butene	24.4±6.0	201.9	29.7	25.2±5.0	275.2	32.4	9.3±2.8	178.5	17.5
3-methyl-1-Butene	12.0±2.4	76.6	11.9	35.6±16.0	332.0	67.2	8.7±5.5	207.0	26.6

2-methyl-1-Butene	16.4±3.3	89.0	16.3	47.4±25.3	1074.0	146.6	17.4±11.4	765.6	73.4
cis-2-Pentene	28.6±5.1	130.4	25.4	34.5±7.9	273.9	46.8	5.5±3.4	130.1	16.4
2-methyl-2-Butene	4.6±1.0	25.8	4.8	37.4±14.6	558.0	84.3	10.2±3.6	139.3	17.5
Butyne	41.0±6.3	171.2	31.5	40.5±12.1	406.7	58.6	18.5±2.8	142.2	18.5
i-Pentane	1809.6±339.6	7793.6	1697.8	827.5±63.3	4646.9	504.0	466.3±33.2	1681.2	254.1
n-Pentane	351.9±63.7	2271.2	318.7	50.1±8.6	416.2	59.9	265.1±25.1	1104.0	192.5
1-Pentene	20.4±5.7	244.3	28.2	50.1±8.6	416.2	59.9	15.6±2.9	182.5	20.3
trans-2-Pentene	15.3±4.1	182.0	20.8	23.6±7.7	302.1	41.4	9.8±4.9	189.6	24.1
2-Methylpentane	268.8±68.7	2253.0	343.6	257.1±29.6	1643.9	237.9	195.5±27.1	1171.6	204.9
n-Hexane	1785.2±547.3	17974.4	2736.1	930.6±147.7	9829.0	1182.2	163.4±23.8	1426.7	182.1
n-Heptane	113.8±39.3	1196.3	196.7	100.2±12.8	877.3	102.4	65.9±5.8	290.7	44.7
n-Octane	42.4±9.6	245.2	48.1	47.5±8.9	739.3	70.4	34.0±3.9	188.0	30.4
2,2-Dimethylbutane	18.7±2.2	64.8	11.3	52.7±8.7	719.6	65.0	20.2±2.0	91.9	14.2
2,3-Dimethylbutane	31.2±17.1	822.5	84.5	68.8±7.1	389.3	55.9	46.3±7.3	311.9	50.0

3-Methylpentane	1911.5±423.0	10292.0	2114.7	172.0±20.5	1260.3	164.4	131.8±18.9	1025.8	144.7
Cyclohexane	66.1±29.1	905.4	145.7	84.1±8.7	601.5	70.3	68.1±8.0	414.4	54.3
2-Methylhexane	49.0±16.4	557.0	82.1	85.7±9.7	429.6	77.5	205.8±19.2	492.8	89.9
3-Methylhexane	172.8±53.5	1651.2	266.3	171.5±19.4	1171.5	155.6	43.7±5.4	271.3	37.0
n-Nonane	29.1±6.4	226.8	32.2	47.6±8.1	621.6	64.4	39.9±7.3	477.2	56.4
n-Decane	457.3±138.9	3680.5	694.4	72.2±15.7	1198.3	126.3	34.0±3.9	188.0	30.4
n-Undecane	71.9±13.6	319.7	65.9	90.8±18.1	1367.5	145.4	--	--	--
Isoprene	270.6±53.0	868.5	264.9	417.0±44.4	1561.0	343.4	409.1±52.5	3122.0	402.0
α-Pinene	261.8±191.5	6810.0	957.3	29.9±4.4	321.5	34.2	21.1±2.9	218.0	22.2
β-Pinene	30.3±10.1	306.4	50.6	53.8±7.3	314.5	57.5	9.9±0.7	32.0	5.4
Benzene	567.0±99.7	3761.2	498.5	493.1±33.2	2308.0	266.3	257.3±14.5	658.2	110.3
Toluene	2878.9±845.3	26556.8	4225.8	1445.3±149.2	6494.2	1196.5	1169.5±229.5	13376.0	1601.8
Ethylbenzene	358.8±63.2	1597.7	316.3	389.1±52.3	4274.0	419.5	193.6±20.7	1350.2	159.1
m/p-Xylene	411.1±82.1	1789.7	410.7	491.8±109.7	10168.0	879.8	299.4±28.4	1600.8	217.9

o-Xylene	168.1±30.0	773.5	150.3	231.3±34.1	2082.0	274.1	151.7±13.7	891.2	105.0
1,3,5-Trimethylbenzene	43.8±8.8	323.5	44.3	38.6±8.4	680.3	67.5	11.6±1.6	125.5	12.7
1,2,4-Trimethylbenzene	177.3±40.1	1527.5	200.6	143.3±25.1	1492.3	201.7	39.6±5.6	336.7	42.9
1,2,3-Trimethylbenzene	64.7±23.8	940.9	117.8	63.1±11.6	809.7	93.4	16.7±3.5	320.3	27.2
i-Propylbenzene	7.4±1.2	38.0	6.3	16.5±1.8	111.1	14.2	7.5±0.7	63.0	5.8
n-Propylbenzene	16.4±2.6	68.9	13.0	34.3±4.3	305.2	34.5	12.4±2.0	188.6	15.3
3-Ethyltoluene	34.6±7.2	212.4	36.1	74.0±10.6	653.0	85.5	24.7±2.9	171.4	22.4
4-Ethyltoluene	18.1±3.4	114.4	17.1	45.4±6.1	429.8	48.7	16.6±2.4	220.2	18.3
2-Ethyltoluene	23.2±4.3	143.0	21.5	40.4±6.7	476.3	53.9	14.0±2.1	186.1	16.3
Formaldehyde	8608.3±1298.0	30244.3	6352.3	2729.0±146.5	6403.5	1123.8	2673.3±283.1	13633.0	2171.5
Acetaldehyde	9853.8±1732.6	46380.0	8198.0	1395.9±81.1	3694.8	622.2	779.4±92.1	3126.0	649.4
Acetone	12786.4±2712.9	75590.0	13131.5	5156.2±421.3	22921.5	3231.7	4995.6±460.6	13370.9	3469.7
Propionaldehyde	--	--	--	325.0±38.2	1593.2	247.0	1547.9±547.2	3071.6	1081.3

Table S6. Comparison of meteorological conditions in the autumns of 2007, 2013 and 2016 (HKO, 2017).

	2007		**2013**		**2016**	
	Mean ± 95%C.I.	Max.	Mean ± 95%C.I.	Max.	Mean ± 95%C.I.	Max.
Temperature (℃)	23.5±0.4	30.0	25.2±0.3	33.9	25.0±0.3	32.7
Relative humidity (%)	64.4±1.4	80.0	58.6±1.3	83.1	77.1±0.7	94.5
Solar radiation (W m^{-2})	190.3±37.7	788.9	159.2±21.3	869.1	119.8±18.2	829.3
Pressure (hPa)	1016.9±0.4	1024.3	1015.0±0.3	1023.1	1012.3±0.3	1020.2
Wind speed at the sampling site (m s^{-1})	2.3±0.2	5.3	1.0±0.1	3.2	0.9±0.1	4.3
Wind speed at HKIA* (m s^{-1})	4.7±0.3	10.8	4.8±0.4	11.7	4.5±0.3	12.4

*HKIA: Hong Kong International Airport.

Table S7. Number of O_3 episode days identified under the tropical cyclone, continental anticyclone and low pressure trough in the autumns of 2007, 2013 and 2016.

Year	Total No. of Episode	Tropical cyclone	Continental anti-cyclone	Low Pressure trough
2007	15*	8 (4 typhoons)	8	1
2013	16	11 (5 typhoons)	5	0
2016	5	4 (3 typhoons)	0	1

*Two O_3 episode days were under the combined influence of tropical cyclone and continental anticyclone.

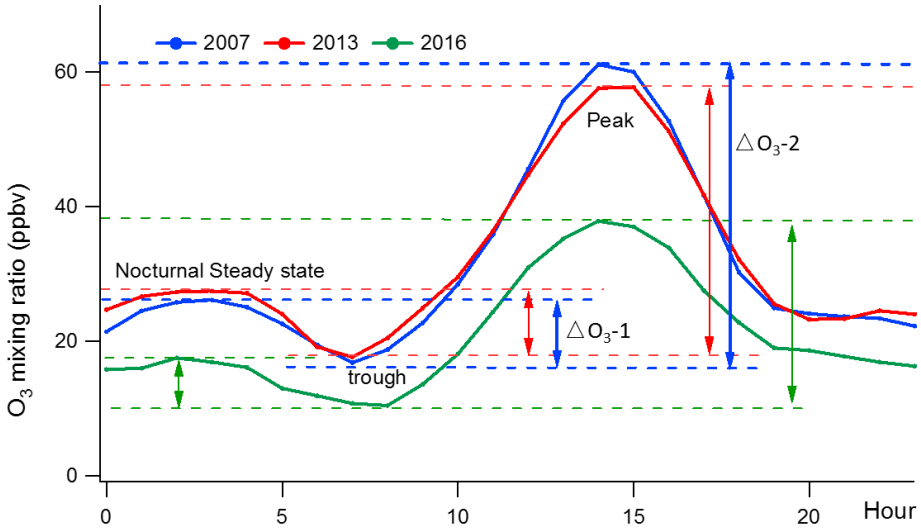

Figure S1. Average diurnal cycles of O_3 in the 2007, 2013 and 2016 sampling campaigns. △O_3-1: O_3 decrease in the early morning driven by NO titration; △O_3-2: photochemically formed O_3 in the daytime (diurnal cycle of O_3 in 2007 as an example).

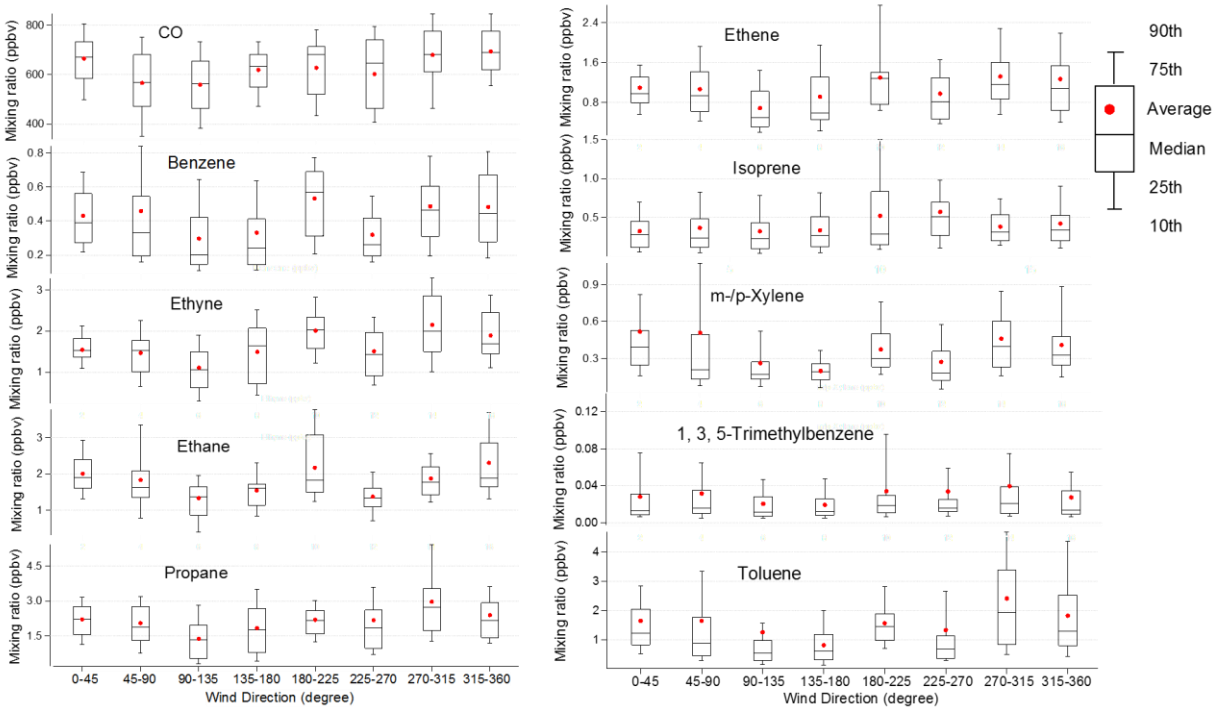

Figure S2. Average mixing ratios of some O_3 precursors in different wind sectors at TC in the three sampling campaigns.

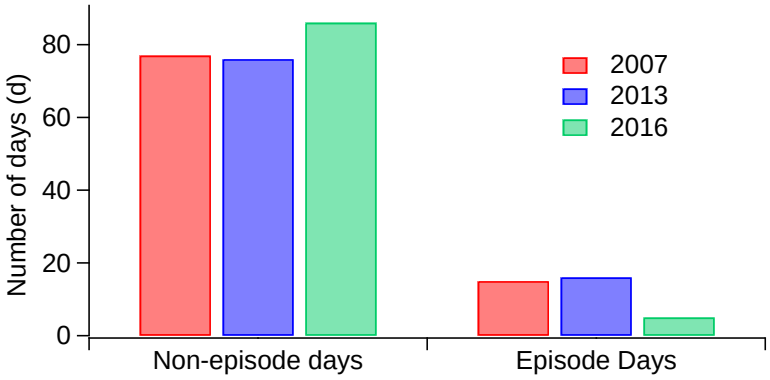

Figure S3. Number of O_3 episode days and non-O_3 episode days in the autumns of 2007, 2013 and 2016.

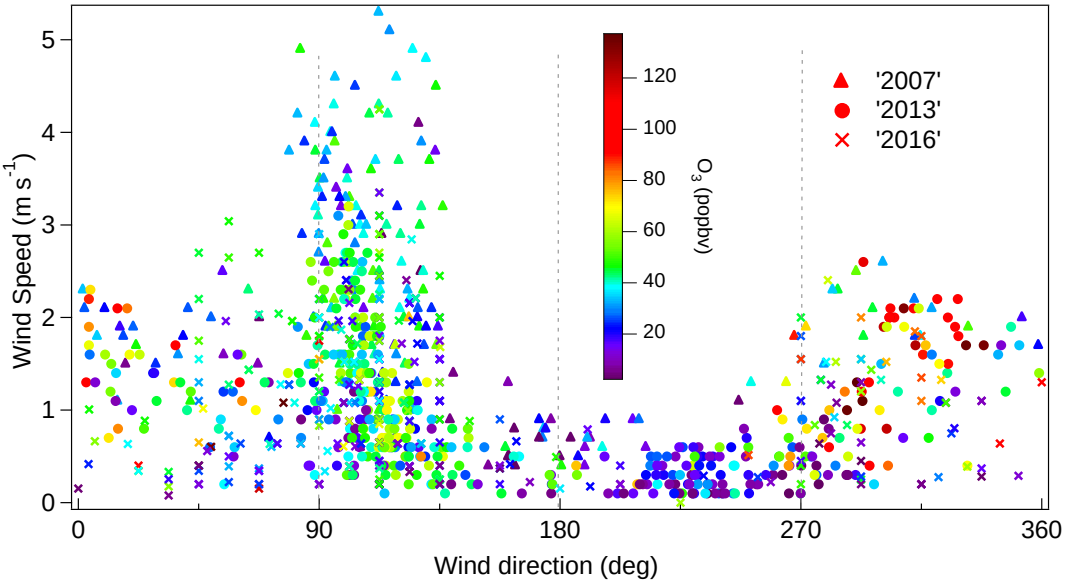

Figure S4. Relationship between the hourly observed O_3 and the wind fields at TC in the three sampling campaigns.

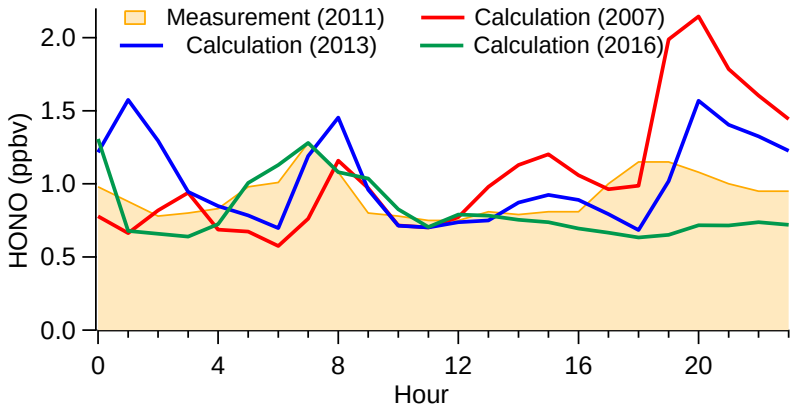

Figure S5. Diurnal cycles of HONO mixing ratios measured at TC in the autumn of 2011 and those calculated from the measured HONO/NO_x ratios and NO_x mixing ratios at the same site in the three sampling campaigns.

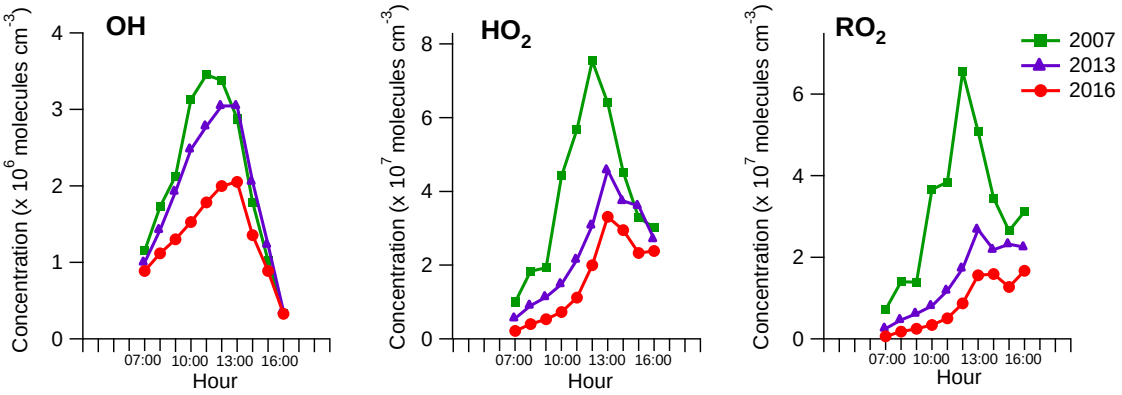

Figure S6. Average diurnal profiles of the simulated OH, HO_2 and RO_2 concentrations on VOC sampling days in 2007, 2013 and 2016. The rebounding of HO_2 and RO_2 concentrations in the late afternoon in 2007 and 2016 were caused by the substantial increases in the concentrations of some VOCs or OVOCs in several samples.

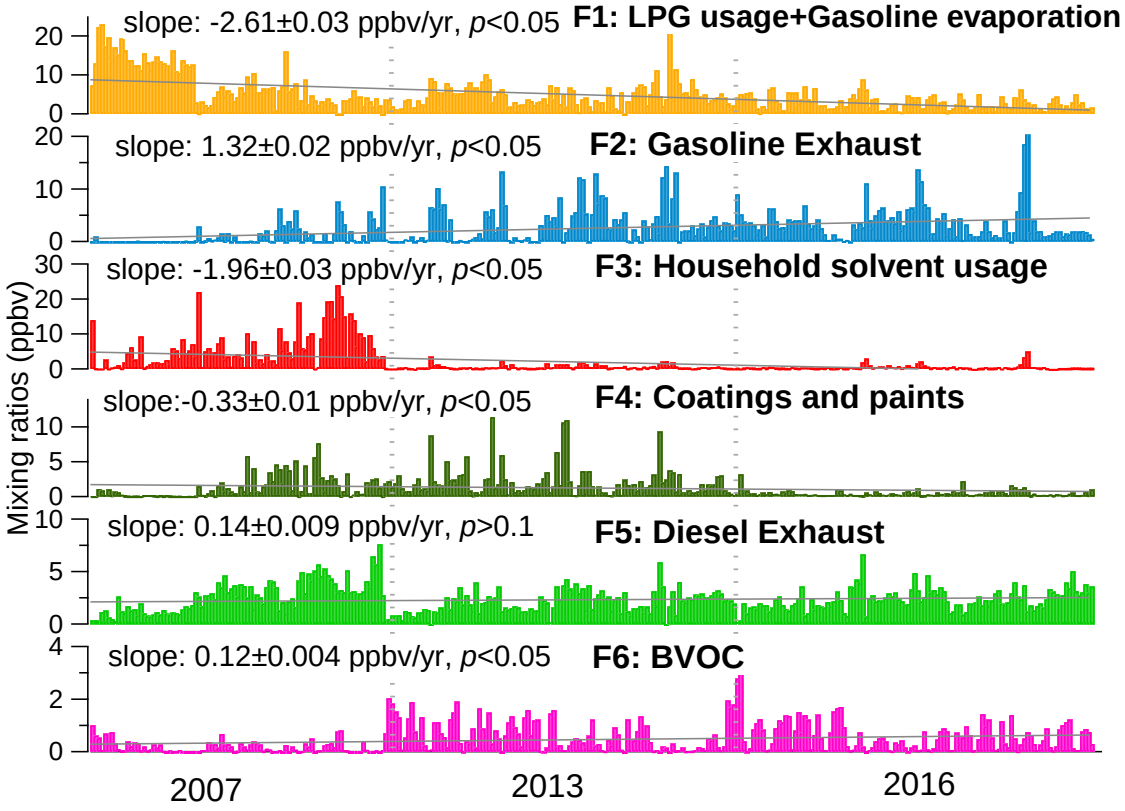

Figure S7. Total mixing ratio of VOCs emitted from each individual source extracted from PMF in the 2007, 2013 and 2016 sampling campaigns. The solid lines represent the linear regressions of the VOC mixing ratios against the sequence number of the samples, with the slope being converted to yearly rates.

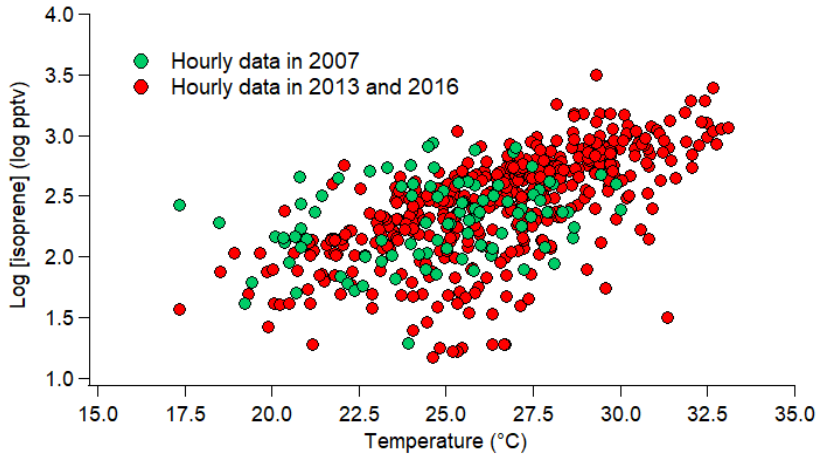

Figure S8. Relationship between the common logarithm of isoprene mixing ratios and temperature.

References

Cheng, H. R., Guo, H., Wang, X. M., Saunders, S. M., Lam, S. H. M., Jiang, F., Wang, T. J., Ding, A. J., Lee, S. C., and Ho, K. F.: On the relationship between ozone and its precursors in the Pearl River Delta: application of an observation-based model (OBM), Environ. Sci. Pollut. Res., 17, 547-560, 2010.

Cheng, H. R., Saunders, S. M., Guo, H., Louie, P. K. K., and Jiang, F.: Photochemical trajectory modeling of ozone concentrations in Hong Kong, Environ. Pollut, 180, 101-110, 2013.

Ding, A. J., Wang, T., Zhao, M., Wang, T. J., and Li, Z. K.: Simulation of sea-land breezes and a discussion of their implications on the transport of air pollution during a multi-day ozone episode in the Pearl River Delta of China, Atmos. Environ., 38, 6737-6750, 2004.

Guo, H., Cheng, H. R., Ling, Z. H., Louie, P. K. K., and Ayoko, G. A.: Which emission sources are responsible for the volatile organic compounds in the atmosphere of Pearl River Delta? J. Hazard. Mater., 188, 116-124, 2011.

Guo, H., Ling, Z. H., Cheung, K., Jiang, F., Wang, D. W., Simpson, I. J., Barletta, B., Meinardi, S., Wang, T. J., Wang, X. M., Saunders, S. M., and Blake, D. R.: Characterization of photochemical pollution at different elevations in mountainous areas in Hong Kong, Atmos. Chem. Phys., 13, 3881-3898, 2013a.

Hong Kong Observatory (HKO): Real-time Data Display from ENVF Atmospheric & Environmental Database, available at: http://envf.ust.hk/dataview/hko_wc/current/ (last access: 25 October 2018), 2017.

Huang, J. P., Fung, J. C., Lau, A. K., and Qin, Y.: Numerical simulation and process analysis of typhoon-related ozone episodes in Hong Kong, J. Geophys. Res. Atmos., 110, D05301, https://doi.org/10.1029/2004jd004914, 2005.

Lam, K. S., Wang, T. J., Wu, C. L., and Li, Y. S.: Study on an ozone episode in hot season in Hong Kong and transboundary air pollution over Pearl River Delta region of China, Atmos. Environ., 39, 1967-1977, 2005.

Lam, S. H. M., Saunders, S. M., Guo, H., Ling, Z. H., Jiang, F., Wang, X. M., and Wang, T. J.: Modelling VOC source impacts on high ozone episode days observed at a mountain summit in Hong Kong under the influence of mountain-valley breezes, Atmos. Environ., 81, 166-176, 2013.

Ling, Z. H., Guo, H., Zheng, J. Y., Louie, P. K. K., Cheng, H. R., Jiang, F., Cheung, K., Wong, L. C., and Feng, X. Q.: Establishing a conceptual model for photochemical ozone pollution in subtropical Hong Kong, Atmos. Environ., 76, 208–220, 2013.

Ling, Z. H. and Guo, H.: Contribution of VOC sources to photochemical ozone formation and its control policy implication in Hong Kong, Environ. Sci. Policy, 38, 180-191, 2014.

Lyu, X. P., Liu, M., Guo, H., Ling, Z. H., Wang, Y., Louie, P. K. K., and Luk, C. W. Y.: Spatiotemporal variation of ozone precursors and ozone formation in Hong Kong: grid field measurement and modelling study, Sci. Total Environ., 569, 1341-1349, 2016a.

Lyu, X. P., Guo, H., Simpson, I. J., Meinardi, S., Louie, P. K. K., Ling, Z. H., Wang, Y., Liu, M., Luk, C. W. Y., Wang, N., and Blake, D. R.: Effectiveness of replacing catalytic converters in LPG-fuelled vehicles in Hong Kong, Atmos. Chem. Phys., 16, 6609-6626, 2016b.

Lyu, X. P., Zeng, L. W., Guo, H., Simpson, I. J., Ling, Z. H., Wang, Y., Murray, F., Louie, P. K. K., Saunders, S. M., Lam, S. H. M., and Blake, D. R.: Evaluation of the effectiveness of air pollution control measure in Hong Kong, Environ. Pollut., 220, 87-94, 2017a.

Lyu, X. P., Guo, H., Wang, N., Simpson, I. J., Cheng, H. R., Zeng, L. W., Saunders, S. M., Lam, S. H. M., Meinardi, S., and Blake, D. R.: Modeling C_1-C_4 alkyl nitrate photochemistry

and their impacts on O_3 production in urban and suburban environments of Hong Kong, J. Geophys. Res. Atmos., 122, 10539-10556, 2017b.

Ou, J.M., Guo, H., Zheng, J.Y., Cheung, K., Louie, P.K.K., Ling, Z.H., and Wang, D.W.: Concentrations and sources of non-methane hydrocarbons (NMHCs) from 2005 to 2013 in Hong Kong: A multi-year real-time data analysis. Atmos. Environ., 103, 196-206, 2015.

Simpson, I. J., Blake, N. J., Barletta, B., Diskin, G. S., Fuelberg, H. E., Gorham, K., Huey, L. G., Meinardi, S., Rowland, F. S., Vay, S. A., Weinheimer, A. J., Yang, M., and Blake, D. R.: Characterization of trace gases measured over Alberta oil sands mining operations: 76 speciated C_2-C_{10} volatile organic compounds (VOCs), CO_2, CH_4, CO, NO, NO_2, NO_y, O_3 and SO_2, Atmos. Chem. Phys., 10, 11931−11954, 2010.

So, K. L. and Wang, T.: On the local and regional influence on ground-level ozone concentrations in Hong Kong, Environ. Pollut., 123, 307-317, 2003.

Wang, Y., Wang, H., Guo, H., Lyu, X. P., Cheng, H. R., Ling, Z. L., Louie, P. K. K., Simpson, I J., Meinardi, S., and Blake, D. R.: Long-term O_3- precursor relationships in Hong Kong: field observation and model simulation, Atmos. Chem. Phys., 17, 10919-10935, 2017.

Wang, Y., Guo, H., Zou, S. C., Lyu, X. P., Ling, Z. H., Cheng, H. R., and Zeren, Y. Z.: Surface O_3 photochemistry over the South China Sea: Application of a near-explicit chemical mechanism box model, Environ. Pollut., 234, 155-166, 2018.

Xu, X., Lin, W., Wang, T., Yan, P., Wang, J., Meng, Z., and Wang, Y.: Long-term trend of surface ozone at a regional background station in eastern China 1991-2006: enhanced variability, Atmos. Chem. Phys., 8, 2595-2607, 2008.

Xu, Z., Wang, T., Wu, J., Xue, L., Chan, J., Zha, Q., Zhou, S., Louie, P. K., and Luk, C. W.: Nitrous acid (HONO) in a polluted subtropical atmosphere: Seasonal variability, direct vehicle

emissions and heterogeneous production at ground surface, Atmos. Environ., 106, 100-109, 2015.

Xue, L. K., Wang, T., Louie, P. K., Luk, C. W., Blake, D. R., and Xu, Z.: Increasing external effects negate local efforts to control ozone air pollution: a case study of Hong Kong and implications for other Chinese cities, Environ. Sci. Technol., 48, 10769-10775, 2014a.

Zhang, J., Wang, T., Chameides, W. L., Cardelino, C., Kwok, J., Blake, D. R., Ding, A., and So, K. L.: Ozone production and hydrocarbon reactivity in Hong Kong, Southern China, Atmos. Chem. Phys., 7, 557-573, 2007.